ROTOR CRACK DETECTION APPROACH USING CONTROLLED SHAFT DEFLECTION

Zbigniew KULESZA*

*Department of Automatic Control and Robotics, Faculty of Mechanical Engineering, Bialystok University of Technology, ul. Wiejska 45C, 15-351 Białystok, Poland

z.kulesza@pb.edu.pl

Abstract: Rotating shafts are important and responsible components of many machines, such as power generation plants, aircraft engines, machine tool spindles, etc. A transverse shaft crack can occur due to cyclic loading, creep, stress corrosion, and other mechanisms to which rotating machines are subjected. If not detected early, the developing shaft crack can lead to a serious machine damage resulting in a catastrophic accident. The article presents a new method for shaft crack detection. The method utilizes the coupling mechanism between the bending and torsional vibrations of the cracked, non-rotating shaft. By applying an external lateral force of a constant amplitude, a small shaft deflection is induced. Simultaneously, a harmonic torque is applied to the shaft inducing its torsional vibrations. By changing the angular position of the lateral force application, the position of the deflection also changes opening or closing of the crack. This changes the way the bending and torsional vibrations are being coupled. By studying the coupled lateral vibration response for each angular position of the lateral force one can assess the possible presence of the crack. The approach is demonstrated with a numerical finite element model of a rotor. The results of the numerical analysis demonstrate the potential of the suggested approach for effective shaft crack detection.

Key words: Rotordynamics, Shaft Crack, Structure Health Monitoring, Diagnosis

1. INTRODUCTION

One of the most dangerous malfunctions of rotating machines are shaft cracks. Transverse cracks occur due to cyclic loading, thermal stresses, creep, corrosion, and other mechanisms to which rotating shafts are subjected. Once a crack has appeared, high stresses develop at its edge and allow the crack to propagate deeper, even if external loads are not changing. When the crack has propagated to a relevant depth, the propagation speed increases dramatically and the shaft may fail in a very short time, what usually leads to a catastrophic accident. That is why an early detection of the potential shaft cracks inside the rotating machine components is so important.

The problems of early shaft crack detection and warning have been in the limelight of many research centers for over 40 years. Different methods have been analyzed, tested and validated experimentally. Generally, the developed approaches can be divided into the vibration based methods and other methods (e.g. ultrasonic, eddy current testing, dye penetrant testing, etc.) (Bachschmid et al., 2010).

Usual crack detection methods are based on vibration signal analysis (Bently and Muszynska, 1986; Gasch, 1993; Grabowski, 1982) for which dynamic signal analyzers, evaluating the fast Fourier transform (FFT) are utilized. By studying the changes in the vibration spectra, the appearance of the possible shaft crack can be easily assessed. The frequently discussed changes in frequency spectra induced by a crack are: a considerable increase of the amplitude of the synchronous frequency 1X and an appearance of its second multiple 2X, especially for a rotor speed near the half of the critical frequency (Bachschmid et al. 2010). However, such symptoms are characteristic not only for cracked rotors, but can be induced by other faults such, as: bearing malfunctions, misalignment, thermal sensitivity, etc. (Bently and Muszynska, 1986).

Other vibration based methods include changes in rotor modal parameters, such as its natural frequencies and mode shapes, which appear in the presence of the developing shaft crack (Bachschmid et al., 2000, 2010).

Nowadays, model-based methods are gaining a special interest. A mathematical model of the analyzed rotor is extensively used here for designing state observers, Kalman filters or the so called robust fault detection filters, which have proved their efficiency not only for shaft crack detection, but also for the determination of its location along the shaft axis (Bachschmid et al., 2000; Isermann, 2005; Kulesza and Sawicki, 2010).

Methods utilizing new signal processing algorithms, such as neural networks, genetic algorithms, wavelets, Huang-Hilbert transform, etc. are also progressing quickly (Guo and Peng, 2007; He at al., 2001; Litak and Sawicki, 2009).

A relatively new approach employs the use of a specially designed diagnostic force applied to the rotating shaft (Ishida and Inoue, 2006; Mani et al., 2005; Sawicki and Lekki, 2008). If the force is harmonic, then the presence of the crack generates responses containing frequencies at combinations of the angular speed, applied forcing frequency, and the rotor natural frequencies. It has been shown, that the appearance of the combinational frequencies is a very strong signature of the shaft crack (Sawicki et al., 2011). However, the research conducted so far has focused on applying the harmonic force, acting in one, fixed direction only.

A well known feature of the cracked shaft is the coupling between the lateral and torsional vibrations. The appearance of coupled bending and torsional vibrations can be utilized as a possible shaft crack indicator, which has been reported by several authors (Darpe et al., 2004; Kiciński, 2005).

Similarly to the previous methods, the present paper recommends the use of an additional diagnostic force applied perpen-

dicularly to the shaft axis. However, the shaft is not rotating, but excited by an additional torque inducing its torsional vibrations. The proposed method is based on vibration signal analysis, namely on the coupling mechanism between the lateral and torsional vibrations.

2. THE CONCEPT OF THE NEW METHOD FOR ROTOR CRACK DETECTION

Schematic diagram explaining the concept of the proposed method is shown in Fig. 1.

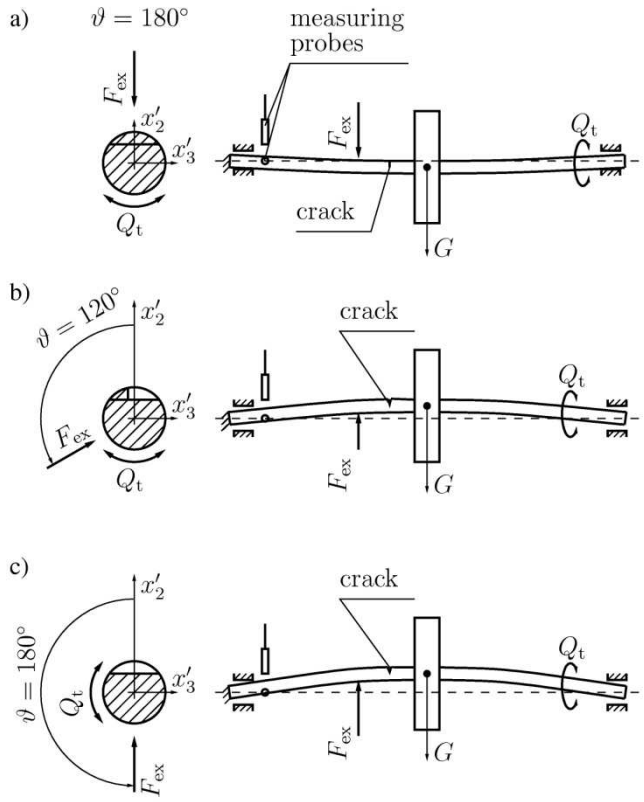

Fig. 1. Schematic diagram of the method for different angular positions ϑ of the external force F_{ex}: a) $\vartheta = 0°$ – fully closed crack, b) $\vartheta = 120°$ – partially open crack, c) $\vartheta = 180°$ – fully open crack

The rotor supported by bearings is not rotating, as one of its ends is fixed to an unmovable base, removing its rotational degree of freedom. The other end is twisted by torque Q_t acting around the axis of the shaft. The amplitude of the torque changes harmonically inducing forced torsional vibrations of the shaft. Simultaneously, an external force F_{ex} of a constant amplitude is applied perpendicularly to the shaft. The force is applied at different angles ϑ, inducing some small deflections of the shaft. By changing the angular position of the force, the position of the deflection also changes opening or closing the crack. This changes the stiffness of the shaft and the way the bending and torsional vibrations are being coupled. It is supposed, that by studying the coupled bending vibration response for each angular position of the external force one will be able to assess the possible presence of the crack.

The suggested method will be tested numerically. For this, the following mathematical models will be formulated: the finite element (FE) model of the rotor, the model of the shaft element with the crack, and the model of crack opening/closing. Based on these models the vibration responses of the cracked rotor for different values and angles of the lateral force as well as for different amplitudes and frequencies of the torsional excitation will be calculated. The Fourier spectra of the vibration responses obtained for both the cracked and uncracked rotors will be used for the comparative study assessing the possible employment of the proposed method for an efficient shaft crack detection.

3. FINITE ELEMENT MODEL OF THE ROTOR

Fig.2 presents the finite element model of the tested rotor.

The rotor consists of a shaft of diameter 16 mm and length 600 mm, and a rigid disk of diameter 120 mm and widtt 30 mm. Two ball bearings located 30 mm from both ends of the shaft are used to support the rotor. Radial stiffness and damping coefficients of the bearings are assumed as $k_b = 3.4 \times 10^6$ N/m and $d_b = 10$ Ns/m. Furthermore, the torsional stiffness and damping coefficients at the left bearing are chosen to be $k_t = 4 \times 10^4$ Nm/rad and $d_t = 20$ Nms/rad, as the left end of the shaft is fixed (Fig. 1). The rotor is made of steel of Young's modulus $E = 2.08 \times 10^{11}$ Pa, Poisson's ratio $v = 0.3$ and density $\rho = 7850$ kg/m^3.

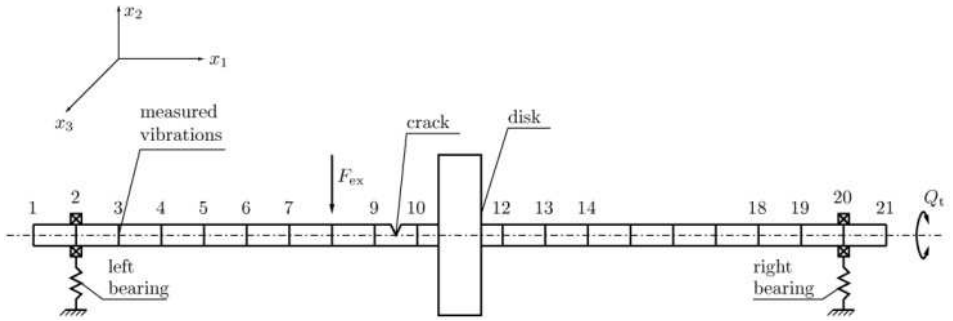

Fig. 2. Finite element model of the tested rotor

The shaft has been divided into 20 finite beam elements (Fig. 2). The 9th element has been assumed as cracked (see: section 4). The bearings are located at the 2nd and 20th node. The external force F_{ex} deflecting the shaft and the additional torque Q_t inducing the torsional vibrations of the rotor are applied at the 8th and the 21st nodes, respectively. The vibration response of the rotor is measured at the 3rd node; bending (along axes x_2 and x_3) and torsional (around axis x_1) vibrations are registered.

Usually, the motion of the rotor is considered in two separate coordinate systems: global (stationary) and local (rotating with a constant angular speed Ω. For the non-rotating rotor fixed with its end to the basis and oscillating around its axis (Fig. 1), only one stationary coordinate system $x_1x_2x_3$ has been assumed, as it is shown in Fig. 3.

Using the finite element method, the motion equations of the rotor can be presented in the following form (Gawroński et al., 1984):

$$\mathbf{M}\ddot{\mathbf{q}} + \mathbf{D}\dot{\mathbf{q}} + \mathbf{K}\mathbf{q} = \mathbf{G} + \mathbf{F}_{\text{ex}} + \mathbf{Q}_{\text{t}} \tag{1}$$

where $\mathbf{M}$ is the mass matrix including the masses and mass moments of inertia of shaft finite elements, rigid disks, etc., $\mathbf{D}$ is the damping matrix and $\mathbf{K}$ is the stiffness matrix (including the stiffness of the cracked shaft finite element). The gyroscopic matrix is not included, as the rotor is not rotating.

Vector $\mathbf{q}$ defines the generalized coordinates of the nodes of the finite element mesh discretizing the shaft. This vector consists of N 6-element sub-vectors, where N is the number of nodes. First three components of each sub-vector are displacements along axes x_1, x_2, x_3, the next three are rotation angles around these axes.

$\mathbf{G}$, $\mathbf{F}_{\text{ex}}$ and $\mathbf{Q}_t$ are vectors of the following generalized forces: gravity, external force perpendicular to the rotor axis, and external torque inducing the oscillations of the rotor.

Mass and stiffness matrices are assembled using the corresponding mass and stiffness sub-matrices of the shaft finite elements, rigid disks, bearings, etc. The damping matrix is usually calculated as a linear combination of the mass and stiffness matrices (the Rayleigh damping). The sub-matrices for rotor elements are given in Appendix A.1. The stiffness matrix for the cracked shaft finite element is discussed in the next sections of this paper.

4. MODEL OF THE CRACK

Usually the crack is modeled by local shaft stiffness changes resulting from the constant opening and closing of the crack. This periodic opening and closing of the crack due to the rotation of the shaft is called the *breathing mechanism*. The first models of the crack accounted for the breathing behavior with only two states, i.e., fully open and fully closed at certain angular position (Gasch, 1993; Grabowski, 1982). These models are defined as *hinge models*. Mayes and Davies (1984) developed a similar model except that the transition from fully open to fully closed is governed by a cosine function depending on shaft rotation angle. Progressive development of the finite element method and its application for rotor dynamics (Nelson and McVaugh, 1976) resulted in more or less complicated models of a variable stiffness cracked shaft finite element. Dimarogonas and Paipetis (1983) derived a full stiffness matrix for a transverse open surface crack on a shaft. Darpe et al. (2004) provided more detail and complete derivations of the flexibility matrix of a cracked rotor segment starting from Castigliano's theorem. They introduced an original model of the crack breathing mechanism, in which the extent of crack opening is determined by calculating the values of compressive stresses at the crack edge.

In the model introduced by Mayes and Davies (1984) shaft stiffness reduction $\Delta\mathbf{K}_{\text{c}}$ for the fully open crack is represented by reductions ΔJ_2, ΔJ_3 of the second moments of area of the shaft cross section around axes x_2 and x_3 at the location of the crack. Different authors (Mayes and Davies, 1984; Sinou and Lees, 2005) provide different formulas for ΔJ_2, ΔJ_3 as the functions of crack depth μ. Here, the relative crack depth μ is defined as $\mu = a/(2R)$, where a is the absolute crack depth and R is the shaft radius (Fig. 3b)).

Consider, for example, the paper of Sinou and Lees (Sinou and Lees, 2005) where:

$$\Delta J_3 = \frac{R^4}{4}\left[(1-\mu)(1-4\mu+2\mu^2)\sqrt{2\mu-\mu^2} + \cos^{-1}(1-\mu)\right]$$
$$\Delta J_2 = \Delta\tilde{J}_2 - \tilde{A}\tilde{X}^2 \tag{2}$$

and

$$\Delta\tilde{J}_2 = \frac{\pi R^4}{4} + R^4\left[\frac{2}{3}(1-\mu)(2\mu-\mu^2)^{3/2} + \frac{1}{4}(1-\mu)(1-4\mu+2\mu^2)\sqrt{2\mu-\mu^2} + \sin^{-1}(\sqrt{2\mu-\mu^2})\right]$$

$$\tilde{A} = R^2\left[(1-\mu)\sqrt{2\mu-\mu^2} + \cos^{-1}(1-\mu)\right]$$

$$\tilde{X} = \frac{2}{3\tilde{A}}R^3(2\mu-\mu^2)^{3/2}$$

After shaft stiffness reduction $\Delta\mathbf{K}_{\text{c}}$ is determined, stiffness matrix $\mathbf{K}_{\text{c}}$ of the cracked element is calculated, as follows (Mayes and Davies, 1984):

$$\mathbf{K}_{\text{c}} = \mathbf{K}_0 - f(\psi)\Delta\mathbf{K}_{\text{c}}, \tag{3}$$

where $\mathbf{K}_0$ is the stiffness matrix of the shaft element with no crack, and $f(\psi)$ is the so called *crack steering function*. Depending on the crack model assumed, the crack steering function $f(\psi)$ takes different forms, e.g. for the hinge model:

$$f(\psi) = \begin{cases} 0, \text{ for } \psi < 0 \\ 1, \text{ for } \psi \geq 0 \end{cases} \tag{4}$$

and for the Mayes and Davies model:

$$f(\psi) = \frac{1}{2}(1-\cos\psi) \tag{5}$$

The argument of these functions is the so called *shaft torsional angle* ψ, or for the simplified models, for which *weight dominance* is assumed, it is the *shaft rotation angle* $\Phi = \Omega t$.

For $f(\psi) = 0$ the crack is fully closed and the stiffness of the cracked element is the same as the stiffness of the uncracked element, i.e. $\mathbf{K}_{\text{c}} = \mathbf{K}_0$. For $f(\psi) = 1$ the crack is fully open, i.e. $\mathbf{K}_{\text{c}} = \mathbf{K}_0 - \Delta\mathbf{K}_{\text{c}}$. For other values the stiffness of the cracked element is somewhere in between these two extreme values.

As can be seen the value of the crack steering function depends only on shaft rotation angle (or on shaft torsional angle). It is sufficient for most cases, where the breathing mechanism of the rotating cracked shaft should be included. However, for the non-rotating shaft, which oscillates harmonically around its axis and is deflected in different angular directions, the presented concept of the crack steering function is insufficient. The extent of crack opening should depend not only on shaft rotation /torsional angle, but also on internal loads at the crack location and resulting internal stresses. As mentioned previously, the method for calculating the extent of crack opening on the

basis of compressive stresses at the crack edge has been introduced by Darpe et al. (2004). Similar approach is used in the present article and is discussed in detail in the next section.

4.1. Stiffness matrix of the cracked shaft element

Figure 3a) presents a shaft element of radius R and length l containing a transverse crack of depth a, located at distance z_c from the i th node. The element is modeled as the finite beam element of six degress of freedom at each node, and loaded with shear forces P_2, P_3, P_8, P_9 bending moments P_5, P_6, P_{11}, P_{12}, torsional moments P_4, P_{10} and axial forces P_1, P_7. According to the Saint-Venant principle, the crack affects the stress field only in the region adjacent to the crack, i.e. only the stiffness matrix of the given finite element is considered.

The cross-section of the shaft element at the location of the crack is presented in Fig. 3b). The uncracked area as well as the closed area of the cracked portion of the cross-section are hatched. The area of the open cracked portion of the cross-section is marked as A_c. The crack is considered as an infinitely thin notch of a half-penny shape. This shape can be limited from the left (or from the right) with the crack left (or right) limit line resulting from its breathing action. This is described in more details in the next section. The positions of the limits are given by b_l and b_r (Fig. 4). The elemental strip of width $d\beta$ and height h, at distance β from shaft axis x_2' is marked on the cross-section. Heights h and α can be calculated, as follows:

$$h = 2\sqrt{R^2 - \beta^2} \qquad \alpha = h - R + a \tag{6}$$

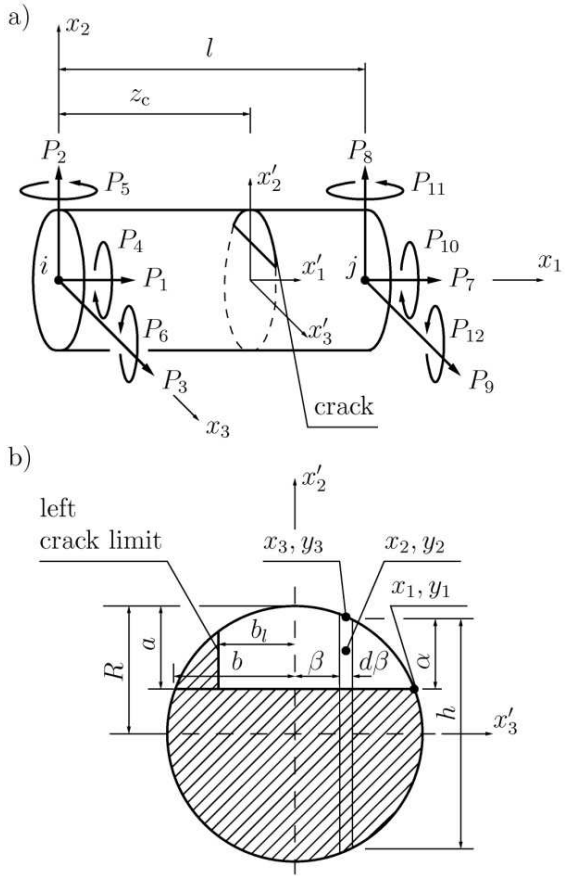

Fig. 3. Cracked shaft finite element: a) acting forces and coordinate systems, b) cracked cross-section

Using Castigliano theorem, the total node displacement q_i in the direction of load P_i can be calculated, as follows (Darpe et al., 2004):

$$q_i = \frac{\partial U_0}{\partial P_i} + \frac{\partial U_c}{\partial P_i} \tag{7}$$

where U_0 is the elastic strain energy of the uncracked element and U_c is the additional strain energy due to the crack. The elastic strain energy U_0 can be presented, as (Darpe et al., 2004):

$$U_0 = \frac{1}{2}\left(\frac{P_1^2 l}{AE} + \frac{\kappa P_2^2 l}{GA} + \frac{P_2^2 l^3}{3EJ_3} + \frac{\kappa P_3^2 l}{GA} + \frac{P_3^2 l^3}{3EJ_2} + \frac{P_4^2 l}{GJ_1} + \frac{P_5^2 l}{EJ_2} + \frac{P_6^2 l}{EJ_3} - \frac{P_2 P_6 l^2}{EJ_3} + \frac{P_3 P_5 l^2}{EJ_2} \right) \tag{8}$$

where E is Young's modulus, G is modulus of rigidity J_1, J_2, J_3 are area moments of inertia around axes x_1, x_2 and x_3, and κ is the shear coefficient.

The additional strain energy due to the crack U_c is given by the following expression (Tada et al., 1973):

$$U_c = \frac{1-\nu}{E} \int_{A_c} \left[\left(\sum_{i=1}^{6} K_{Ii} \right)^2 + \left(\sum_{i=1}^{6} K_{IIi} \right)^2 + (1+\nu) \left(\sum_{i=1}^{6} K_{IIIi} \right)^2 \right] dA_c \tag{9}$$

where A_c is the area of the open cracked portion of the shaft cross-section (Fig. 4), ν is the Poisson's ratio, and K_{Ii}, K_{IIi}, K_{IIIi} are stress intensity factors (SIFs) corresponding to three different modes of crack displacement: opening (I), sliding (II) and shearing (III).

The nonzero SIFs take the following forms (Tada et al., 1973):

$$K_{II} = \frac{P_1}{\pi R^2}\sqrt{\pi\alpha}F_1, \quad K_{I5} = \frac{4(P_5 + P_3 z_c)\beta}{\pi R^4}\sqrt{\pi\alpha}F_1$$

$$K_{I6} = \frac{2(P_2 z_c - P_6)h}{\pi R^4}\sqrt{\pi\alpha}F_2, \quad K_{II2} = \frac{\kappa P_2}{\pi R^2}\sqrt{\pi\alpha}F_{II} \tag{10}$$

$$K_{III3} = \frac{\kappa P_3}{\pi R^2}\sqrt{\pi\alpha}F_{III}, \quad K_{III4} = \frac{P_4 h}{\pi R^4}\sqrt{\pi\alpha}F_{III}$$

where the correction functions F_1, F_2, F_{II}, F_{III} are defined, as follows (Tada et al., 1973):

$$F_1 = F_{III}\frac{0.752 + 2.02\mu + 0.37(1-\sin\lambda)^3}{\cos\lambda}$$

$$F_2 = F_{III}\frac{0.923 + 0.199(1-\sin\lambda)^4}{\cos\lambda}$$

$$F_{II} = \frac{1122 - 0561\mu + 0085\mu^2 + 018\mu^3}{\sqrt{1-\mu}}, \quad F_{III} = \sqrt{\frac{\tan\lambda}{\lambda}}$$

where: $\mu = \frac{\alpha}{h}, \lambda = \frac{\pi\alpha}{2h}$.

Integrating Eqs. (8) and (9) with Eqs. (7) and (10), the generalized coordinates q_i can be presented in the following matrix form

$$\mathbf{q} = \mathbf{G}_c \mathbf{P} \tag{11}$$

where $\mathbf{q} = [q_1 \quad q_2 \quad \cdots \quad q_6]^T$, $\mathbf{P} = [P_1 \quad P_2 \quad \cdots \quad P_6]^T$ and $\mathbf{G}_c$ is the symmetric 6×6 flexibility matrix. The nonzero elements

of this matrix are given in Appendix 2. As can be seen the non-zero elements are located not only at the main diagonal, but also above and below it (e.g. $g_{2,4}$, $g_{3,4}$, $g_{3,1}$). It is obvious that these elements will couple the bending, axial and torsional vibrations. However, the off-diagonal, nonzero elements are present only in the flexibility matrix of the cracked shaft element. The other shaft finite elements do not contain the nonzero elements beyond the main diagonal (Appendix 1).

Considering the static equilibrium condition, 12 generalized coordinates of the cracked shaft finite element can be obtained (Przemieniecki, 1968):

$$\begin{bmatrix} q_1 & q_2 & \dots & q_{12} \end{bmatrix}^T = \mathbf{T}\begin{bmatrix} q_1 & q_2 & \dots & q_6 \end{bmatrix}^T \tag{12}$$

where $\mathbf{T} = [\mathbf{I}, \mathbf{T}_s]^T$ is the 12×6 transformation matrix, I is the identity matrix, and the nonzero elements of the 6×6 matrix $\mathbf{T}_s$ are, as follows:

$$t_{s1,1} = t_{s2,2} = t_{s3,3} = t_{s4,4} = t_{s5,5} = t_{s6,6} = -1\,,\; t_{s2,6} = -t_{s3,5} = l$$

The flexibility matrix $\mathbf{G}_c$ can be used to find the stiffnes matrix $\mathbf{K}_c$ of the cracked shaft finite element:

$$\mathbf{K}_c = \mathbf{T}\mathbf{G}_c\mathbf{T}\,. \tag{13}$$

4.2. Crack breathing mechanism

The changes in the extent of crack opening can be presented in terms of changes of circular segment area A_c inside the cross section of the cracked element (Fig. 4). Depending on external loads, this area changes from zero (for the fully closed crack) to its maximum value (for the fully open crack). Thus, the limits b_l and b_r separating cracked and uncracked portions of this area from the left and from the right, change from $-b$ to b (for left limit b_l) and from b to $-b$ (for right limit b_r). Here, b denotes half of the crack edge width. As can be seen from the lower part of Fig. 4, only one limit (left or right) can change at the same time, but not both. This way, the integration limits for the flexibility matrix $\mathbf{G}_c$ (Eq. 11) change in time. Consequently, the stiffness matrix K_c (Eq. 13) also changes in time, simulating the breathing behavior of the crack.

To determine the locations of the left b_l and right b_r limits, the generalized forces $\mathbf{P}_w$ acting at the nodes of the cracked shaft element should be be evaluated at each time step. These forces can be calculated using the generalized coordinates $\mathbf{q}_w$ and the stiffness matrix $\mathbf{K}_c$ of the cracked element

$$\mathbf{P}_w = \mathbf{K}_c\mathbf{q}_w \tag{14}$$

Vector of nodal coordinates $\mathbf{q}_w$ can be obtained from the vibration response $\mathbf{q}$ of the rotor by solving the motion equations (1). The nodal forces $\mathbf{P}_w$ are used in Eq. 10 to calculate stress intensity factors along the crack edge. For this, the crack edge is divided into a given number of equally spaced points at which the SIFs are evaluated. In practice only K_{I1}, K_{I5}, K_{I6} stress intensity factors are accounted for, as only they are responsible for the opening mode crack displacement influencing the extent of crack opening. To simplify, not separate SIFs are analyzed, but their sum K_s, where:

$$K_s = K_{I1} + K_{I5} + K_{I6} \tag{15}$$

A negative sign of K_s indicates compressive stress and the closed crack at a given point of the crack edge. Similarly, a positive sign of K_s indicates tensile stress and the open state of the crack at a given point of the crack edge. Thus, analyzing the sign of the overall stress intensity factor K_s at each point of the crack edge, the locations of the left b_l or right b_r crack limit can be determined. Once the crack limits are ascertained the flexibility $\mathbf{G}_c$ and stiffness $\mathbf{K}_c$ matrices are updated (Eqs. 11) and 13), and the global stiffness matrix $\mathbf{K}$ is assembled.

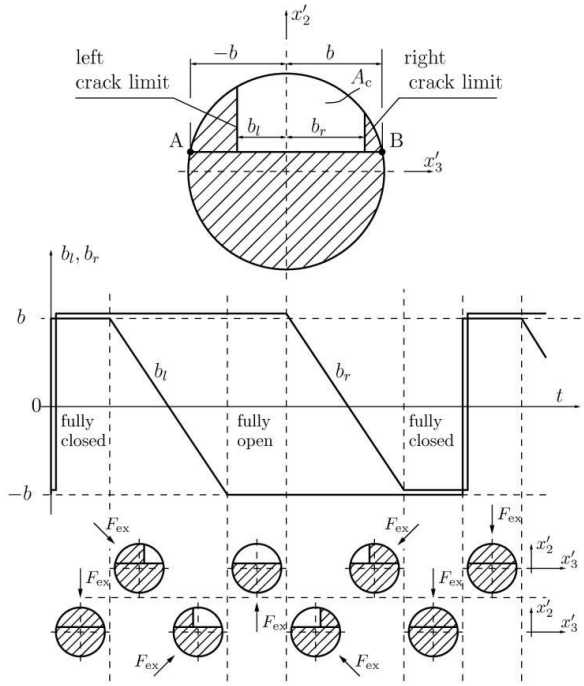

Fig. 4. Crack breathing mechanism

Next, from Eq. 1 the rotor response $\mathbf{q}$ is evaluated for the new time step, and the vector of nodal coordinates is extracted from it. Again, using Eq. 14, the vector of nodal forces is obtained, and the overall SIF K_s at several points along the crack edge is calculated. Based on the sign of K_s the new locations b_l and b_r of crack limits are evaluated and stiffness matrix $\mathbf{K}_c$ is updated. This way, at every iteration step, the overall stiffness matrix $\mathbf{K}$ of the rotor is updated by reevaluating the stiffness matrix $\mathbf{K}_c$ of the cracked finite element.

5. RESULTS

During the numerical analysis, three different models of the rotor have been considered: the first with no crack, the second with a 25% deep crack and the third with a 40% deep crack. In all cases the value of the lateral force was $F_{ex} = 100$ N, while the form of the external torque $Q_t = A_Q \sin(2\pi f_Q t)$, where the amplitude $A_Q = 500$ Nm. Two different frequencies of the exciting torque have been considered: $f_Q = 60$ Hz and $f_Q = 80$ Hz.

Using stiffness $\mathbf{K}$, damping $\mathbf{D}$, and mass $\mathbf{M}$ matrices (Eq. (1)), the natural frequencies of the rotor have been evaluated. The first two bending frequencies are located at $f_n = 40.6$ Hz and $f_n = 166.1$ Hz, while the first torsional frequency is at $f_t = 612.3$ Hz.

Motion equations (1) are solved using the Newmark integration scheme (Newmark, 1959), which is more efficient for large systems. The equations are integrated until a steady state has been established and then the FFT is calculated.

Figs. 5-12 present frequency responses for different angles ϑ of the lateral force $\mathrm{F_{ex}}$. Bending response is shown only for the vertical $\mathrm{x_2}$ axis, as the vibrations along axes $\mathrm{x_2}$ and $\mathrm{x_3}$ are much the same.

Figs. 5 and 6 present torsional and bending responses of the uncracked rotor. As expected, the torsional spectrum contains only one component of the exciting torque frequency $f_Q = 60$ Hz. In the bending response only the first natural frequency $f_n = 40.6$ Hz is slightly induced. Such characteristics are typical for the linear model of the rotor.

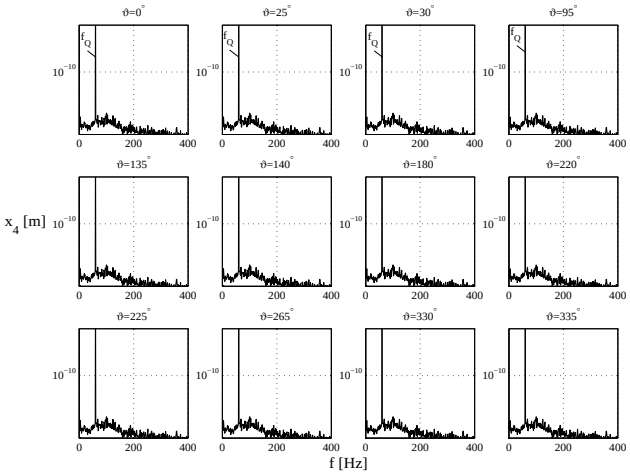

Fig. 5. Torsional response for different angles ϑ; uncracked shaft; $f_Q = 60$ Hz

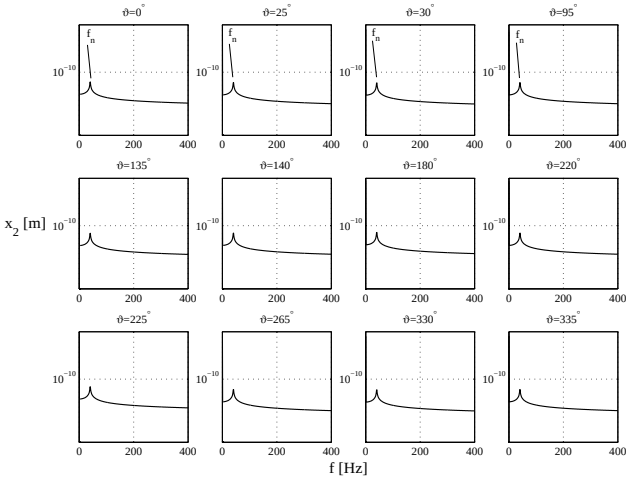

Fig. 6. Bending response for different angles ϑ; uncracked shaft; $f_Q = 60$ Hz

Figs. 7, 8 and 9 present responses of the 25% cracked rotor. Due to the nonlinearities introduced by the crack subsequent integer multiples of the exciting torque frequency $f_Q = 60$ Hz denoted as 2X (120 Hz), 3X (180 Hz), 4X (240 Hz), 5X (300 Hz), and several other frequencies of the same high amplitudes of 10^{-7} rad appear in the torsional response (Fig. 7). However, all these frequencies are observed only for particular angles ϑ, i.e. for ϑ from $30°$ to $135°$ and for ϑ from $225°$ to $330°$. It should be noticed, that such angle ranges correspond to the situations, when the crack is partially open. For other ranges, only one component is present in the vibration spectra. This is the frequency of the exciting torque $f_Q = 60$ Hz. In this case, the angles are near $0°$ and $180°$, what corresponds to the (almost) fully open and (almost) fully closed crack.

The similar, yet more important situation, is in the bending spectra (Figs. 8 and 9), where for the same angle ranges the same frequency components can be observed (including the multiples 2X, 3X, 4X, 5X, and so on). For other angle ranges, the bending frequency spectrum contains only slightly induced: natural frequency $f_n = 40.6$ Hz and exciting torque frequency $f_Q = 60$ Hz (or $f_Q = 80$ Hz).

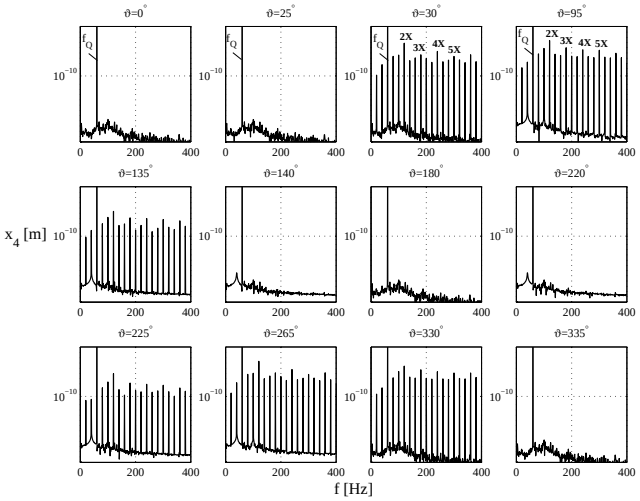

Fig. 7. Torsional response for different angles ϑ; 25% crack; $f_Q = 60$ Hz

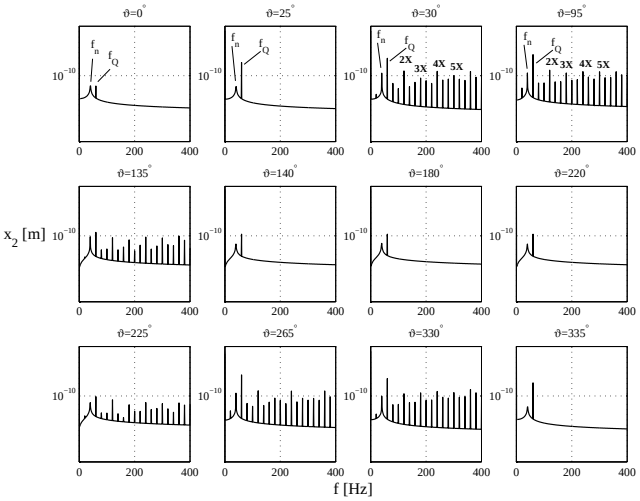

Fig. 8. Bending response for different angles ϑ; 25% crack; $f_Q = 60$ Hz

The rotor with a 40% deep crack behaves similarly (Figs. 10, 11, and 12), yet the angle ranges for which additional bending frequencies are induced are wider: from $\vartheta = 20°$ to $\vartheta = 140°$ and from $\vartheta = 210°$ to $\vartheta = 340°$. This would suggest, that for deeper cracks it is more difficult to completely close (or completely open) the crack and consequently not to induce the additional bending frequencies. Nevertheless, for the 40% deep crack the angle ranges with the differences in the frequency responses

are evident. Presumably, such crack signatures can be used for the efficient diagnosis of the health of the machine.

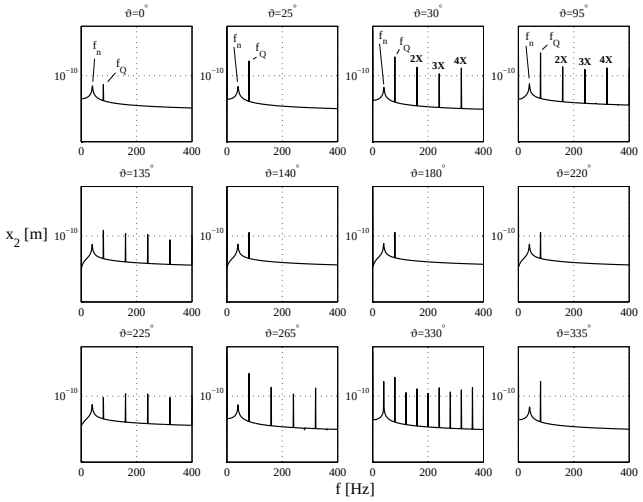

Fig. 9. Bending response for different angles ϑ; 25% crack; $f_Q = 80$ Hz

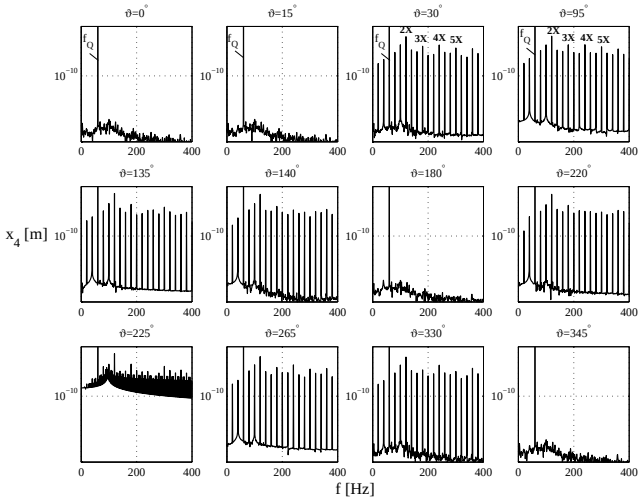

Fig. 10. Torsional response for different angles ϑ; 40% crack; $f_Q = 60$ Hz

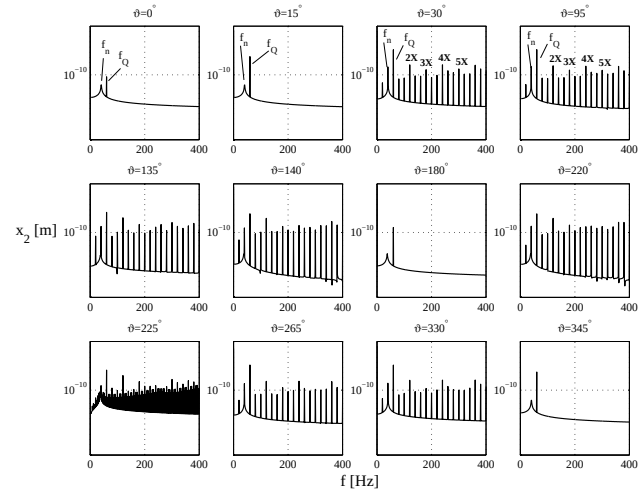

Fig. 11. Bending response for different angles ϑ; 40% crack; $f_Q = 60$ Hz

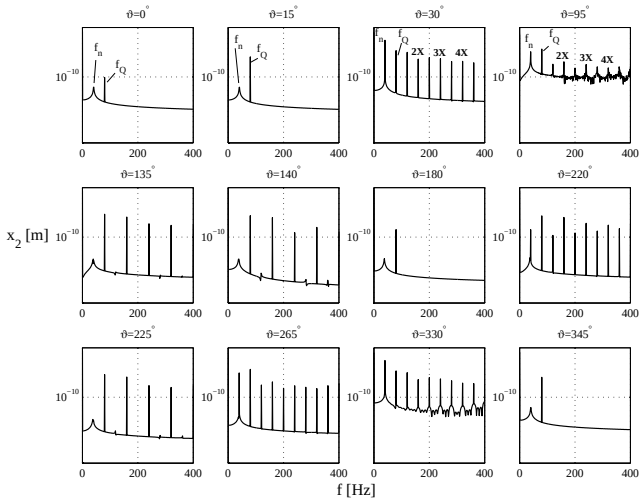

Fig. 12. Bending response for different angles ϑ; 40% crack; $f_Q = 80$ Hz

6. CONCLUSIONS

Early crack detection is a serious problem, as small shaft stiffness changes due to the crack have little influence on the rotor vibration response. During the normal machine operation the changes in the rotor response are small and practically unmeasurable. Hence, the methods amplifying the rotor sensitivity to the crack appearance and propagation should be applied.

One of these methods is suggested in the present article. Inducing the deflection of the non-rotating shaft excited by the forced torsional vibrations, the coupled bending vibrations are induced. The maximum amplification and the appearance of the multiples of the torsional frequency in the bending spectrum are observed if the deflection is induced in a direction opening the crack partially. On the other hand, the minimum coupled bending amplitudes are observed if the deflection is directed in a way ensuring the fully opening or closing of the crack. Such behavior can be explained by the fact, that in a case of a partially open crack, the multiples of the forced frequency appear quite naturally in the torsional spectrum. These frequencies are transformed by the off-diagonal non-zero elements of the stiffness matrix to the coupled bending vibrations resulting in the same multiples in the bending vibration spectra. The coupling between the bending and torsional vibrations takes place only if the cracked shaft is considered, as only then the off-diagonal non-zero elements appear in the stiffness matrix.

Numerical results confirm the potential of the proposed method. The changes in coupled bending vibrations are observed only for the cracked shaft. However, further analysis is needed to determine the required value of the external force inducing the shaft deflection, the amplitude and frequency of the exciting torque generating the forced torsional vibrations, the location of these forces along the shaft length, the location of the measuring probes, etc. At the same time, the experimental verification of the proposed method should also be conducted.

Future extension of the proposed method may involve its application for the rotating shafts. This would enable the continuous monitoring of the rotor's health, without the need to switch the machine off its normal operation.

REFERENCES

1. **Bachschmid N., Pennacchi P., Tanzi E.** (2010), *Cracked rotors: a survey on static and dynamic behaviour including modelling and diagnosing*, Springer-Verlag Berlin Heidelberg.
2. **Bachschmid N., Pennacchi P., Tanzi E., Vania A.** (2000), Identification of transverse crack position and depth in rotor systems, *Meccanica*, 35, 563-582.
3. **Bently D. E., Muszynska A.** (1986), Detection of rotor cracks, *Proceedings of Texas A&M University 15th Turbomachinery Symposium and Short Courses*, Corpus Christi, TX, 129-139.
4. **Darpe A. K., Gupta K., Chawla A.** (2004), Coupled bending, longitudinal and torsional vibrations of a cracked rotor, *Journal of Sound and Vibration*, 269, 33-60.
5. **Dimarogonas A.D., Paipetis S.A.** (1983), *Analytical Methods in Rotor Dynamics,* Applied Science Publishers, London.
6. **Gasch R.** (1993), A survey of the dynamic behavior of a simple rotating shaft with a transverse crack, *Journal of Sound and Vibration*, 160 (2), 313-332.
7. **Gawroński W., Kruszewski J., Ostachowicz W., Tarnowski J., Wittbrodt E.** (1984), *Finite element method in dynamics of structures*, Arkady, Warsaw (in Polish).
8. **Grabowski B.** (1982), Shaft vibrations in turbomachinery excited by cracks, In proceedings of the 2nd Workshop on Rotordynamic Instability Problems in High-performance Turbomachinery, Texas A&M University, *NASA Conference Publication*, 2250, 81-97.
9. **Guo D., Peng Z. K.** (2007), Vibration analysis of a cracked rotor using Hilbert-Huang transform, *Mechanical Systems and Signal Processing*, 21, 3030-3041.
10. **He Y., Guo, D., Chu, F.** (2001), Using genetic algorithms to detect and configure shaft crack for rotor-bearing system, *Computer Methods in Applied Mechanics and Engineering*, 190, 5895-5906.
11. **Isermann R.** (2005), Model-based fault detection and diagnosis – status and applications, *Annual Reviews in Control*, 29, 71-85.
12. **Ishida Y., Inoue T.** (2006), Detection of a rotor crack using a harmonic excitation and nonlinear vibration analysis, *ASME Journal of Vibration and Acoustics*, 128, 741-749.
13. **Kiciński J.** (2005), Dynamics of rotors and slide bearings, *Fluid Flow Machinery Series*, Vol. 28, IMP PAN, Gdansk (in Polish).
14. **Kulesza Z., Sawicki J. T.** (2010), Auxiliary state variables for rotor crack detection, *Journal of Vibration and Control*, 17 (6), 857-872.
15. **Litak G., Sawicki J. T.** (2009), Intermittent behaviour of a cracked rotor in the resonance region, *Chaos, Solitions and Fractals*, 42, 1495-1501.
16. **Mani G., Quinn D. D., Kasarda M.** (2005), Active health monitoring in a rotating cracked shaft using active magnetic bearings as force actuators, *Journal of Sound and Vibration*, 294, 454-465.
17. **Mayes, I. W. and Davies, W. G. R.** (1984), Analysis of the response of a multi-rotor-bearing system containing a transverse crack in a rotor, *Journal of Vibration, Acoustics, Stress and Reliability in Design*, 83, DET 84, 139-145.
18. **Nelson H. D., McVaugh J. M.** (1976), The dynamics of rotor bearing systems using finite elements, *ASME Journal of Engineering for Industry*, 98, 593-600.
19. **Newmark N. M.** (1959), A method of computation for structural dynamics, *ASCE Journal of Engineering Mechanics Division*, 85, 67-94.
20. **Przemieniecki J. S.** (1968), *Theory of matrix structural analysis*, Mc Graw-Hill, New York.
21. **Sawicki J. T., Friswell M. I., Kulesza Z., Wroblewski A., Lekki J. D.** (2011), Detecting cracked rotors using auxiliary harmonic excitation, *Journal of Sound and Vibration,* 330, 1365-1381.
22. **Sawicki J. T., Lekki J. D.** (2008), Smart structural health monitoring of rotating components using active magnetic force actuators, *Proceedings of NASA Aviation Safety Technical Conference*, Denver, Colorado, 1-23.
23. **Sinou J-J., Lees A.W.** (2005), The influence of cracks in rotating shafts, *Journal of Sound and Vibration*, 285, 1015-1037.
24. **Tada H., Paris P. C., Irwin G. R.** (1973), *The stress analysis of cracks handbook*, Del Research Corporation, Hellertown, PA.

This study is supported by the research project No S/WM/1/2012.

APPENDIX 1

Elemental matrices of the finite element model of the rotor have been obtained on the basis of (Gawroński et al., 1984).

Mass matrix of shaft finite element is, as follows:

$$\mathbf{M} = \rho l \begin{bmatrix} m_{1,1} & m_{1,2} & m_{1,3} & m_{1,4} & \dots & m_{1,11} & m_{1,12} \\ & m_{2,2} & m_{2,3} & m_{2,4} & \dots & m_{2,11} & m_{2,12} \\ & & m_{3,3} & m_{3,4} & \dots & m_{3,11} & m_{3,12} \\ & & & \dots & \dots & \dots & \dots \\ & & & & & m_{11,11} & m_{11,12} \\ symm. & & & & & & m_{12,12} \end{bmatrix}$$

where the nonzero elements lying on and above the main diagonal are, as follows:

$$m_{1,1} = \frac{A}{3},\ m_{1,7} = \frac{A}{6},\ m_{2,2} = \frac{13A}{35} + \frac{6J_3}{5l^2}$$

$$m_{2,6} = \frac{11Al}{210} + \frac{J_3}{10l},\ m_{2,8} = \frac{9A}{70} - \frac{J_3}{5l^2}$$

$$m_{2,12} = \frac{-13Al}{420} + \frac{J_3}{10l},\ m_{3,3} = \frac{13A}{35} + \frac{6J_2}{5l^2}$$

$$m_{3,5} = \frac{-11Al}{210} - \frac{J_2}{10l},\ m_{3,9} = \frac{9A}{70} - \frac{6J_2}{5l^2}$$

$$m_{3,11} = \frac{13Al}{420} - \frac{J_2}{10l},\ m_{4,4} = \frac{J_1}{3},\ m_{4,10} = \frac{J_1}{6}$$

$$m_{5,5} = \frac{Al^2}{105} + \frac{2J_2}{15},\ m_{5,9} = -m_{3,11}$$

$$m_{5,11} = \frac{-Al^2}{140} - \frac{J_2}{30},\ m_{6,6} = \frac{Al^2}{105} + \frac{2J_3}{15},\ m_{6,8} = -m_{2,12}$$

$$m_{6,12} = \frac{-Al^2}{140} - \frac{J_3}{30},\ m_{7,7} = m_{1,1},\ m_{8,8} = m_{2,2}$$

$$m_{8,12} = -m_{2,6},\ m_{9,9} = m_{3,3},\ m_{9,11} = -m_{3,5}$$

$$m_{10,10} = m_{4,4},\ m_{11,11} = m_{5,5},\ m_{12,12} = m_{6,6}$$

Stiffness matrix of shaft finite element takes the following form:

$$\mathbf{K} = \frac{E}{l} \begin{bmatrix} k_{1,1} & k_{1,2} & k_{1,3} & k_{1,4} & \dots & k_{1,11} & k_{1,12} \\ & k_{2,2} & k_{2,3} & k_{2,4} & \dots & k_{2,11} & k_{2,12} \\ & & k_{3,3} & k_{3,4} & \dots & k_{3,11} & k_{3,12} \\ & & & \dots & \dots & \dots & \dots \\ & & & & & k_{11,11} & k_{11,12} \\ sym. & & & & & & k_{12,12} \end{bmatrix}$$

where the nonzero elements lying on and above the main diagonal are, as follows:

$$k_{1,1} = A\ ,\ k_{1,7} = -k_{1,1}\ ,\ k_{2,2} = \frac{12J_3}{l^2}\ ,\ k_{2,6} = \frac{6J_3}{l}$$

$$k_{2,8} = -k_{2,2}\ ,\ k_{2,12} = k_{2,6}\ ,\ k_{3,3} = \frac{12J_2}{l^2}\ ,\ k_{3,5} = \frac{-6J_2}{l}$$

$$k_{3,9} = -k_{3,3}\ ,\ k_{3,11} = k_{3,5}\ ,\ k_{4,4,} = \frac{J_1}{2(1+\nu)}\ ,\ k_{4,10} = -k_{4,4}$$

$$k_{5,5} = 4J_2\ ,\ k_{5,9} = -k_{3,5}\ ,\ k_{5,11} = 2J_2\ ,\ k_{6,6} = 4J_3$$

$$k_{6,8} = -k_{2,6}\ ,\ k_{6,12} = 2J_3\ ,\ k_{7,7} = k_{1,1}\ ,\ k_{8,8} = k_{2,2}$$

$$k_{8,12} = -k_{2,6}\ ,\ k_{9,9} = k_{3,3}\ ,\ k_{9,11} = k_{3,5}\ ,\ k_{10,10} = k_{4,4}$$

$$k_{11,11} = k_{5,5}\ ,\ k_{12,12} = k_{6,6}$$

Damping matrix $\mathbf{D}$ of shaft finite element is calculated, as: $\mathbf{D} = \alpha_{\mathrm{d}}\mathbf{K} + \beta_{\mathrm{d}}\mathbf{M}$, where the following values have been assumed: $\alpha_{\mathrm{d}} = 1 \times 10^{-5}, \beta_{\mathrm{d}} = 0$.

Mass matrix of a disk takes the following form: $\mathbf{M} = \mathrm{diag}(m, m, m, J_{m1}, J_{m2}, J_{m3})$, where m is the mass of the disk, and J_{m1}, J_{m2}, J_{m3} are mass moments of inertia of the disk around x_1, x_2, and x_3 axes.

Stiffness matrix of a bearing takes the following form: $\mathbf{K} = \mathrm{diag}(k_a, k_b, k_b, k_t, 0, 0)$, where k_a, k_b, k_t are stiffness coefficients for axial, bending and torsional displacements.

Damping matrix of the bearing takes the following form: $\mathbf{D} = \mathrm{diag}(d_a, d_b, d_b, d_t, 0, 0)$, where d_a, d_b, d_t are damping coefficients for axial, bending and torsional speeds.

APPENDIX 2

Flexibility matrix G_{c} of the cracked shaft element can be presented, as:

$$\mathbf{G}_{\mathrm{c}} = \begin{bmatrix} g_{1,1} & g_{1,2} & \cdots & g_{1,6} \\ & g_{2,2} & \cdots & g_{2,6} \\ & & \cdots & \cdots \\ sym. & & & g_{6,6} \end{bmatrix}$$

where the nonzero elements lying on and above the main diagonal are, as follows:

$$g_{1,1} = \frac{l}{AE} + \frac{2}{\pi E' R^4}\int_{A_{\mathrm{c}}} \alpha F_1^2 dA_{\mathrm{c}}\ ,\quad g_{1,2} = \frac{4z_{\mathrm{c}}}{\pi E' R^6}\int_{A_{\mathrm{c}}} \alpha h F_1 F_2 dA_{\mathrm{c}}$$

$$g_{1,3} = \frac{8z_{\mathrm{c}}}{\pi E' R^6}\int_{A_{\mathrm{c}}} \alpha\beta F_1^2 dA_{\mathrm{c}}$$

$$g_{1,5} = \frac{8}{\pi E' R^6}\int_{A_{\mathrm{c}}} \alpha\beta F_1^2 dA_{\mathrm{c}}\ ,\ g_{1,6} = \frac{-4}{\pi E' R^6}\int_{A_{\mathrm{c}}} \alpha h F_1 F_2 dA_{\mathrm{c}}$$

$$g_{2,2} = \left(\frac{\kappa l}{GA} + \frac{l^3}{3EJ_2}\right) + \frac{8z_{\mathrm{c}}^2}{\pi E' R^8}\int_{A_{\mathrm{c}}} \alpha h^2 F_2^2 dA_{\mathrm{c}} + \frac{2\kappa^2}{\pi E' R^4}\int_{A_{\mathrm{c}}} \alpha F_{\mathrm{II}}^2 dA_{\mathrm{c}}$$

$$g_{2,3} = \frac{16z_{\mathrm{c}}^2}{\pi E' R^8}\int_{A_{\mathrm{c}}} \alpha\beta h F_1 F_2 dA_{\mathrm{c}}$$

$$g_{2,4} = \frac{4\kappa}{\pi E' R^6}\int_{A_{\mathrm{c}}} \alpha\beta F_{\mathrm{II}}^2 dA_{\mathrm{c}}$$

$$g_{2,5} = \frac{16z_{\mathrm{c}}}{\pi E' R^8}\int_{A_{\mathrm{c}}} \alpha\beta h F_1 F_2 dA_{\mathrm{c}}$$

$$g_{2,6} = -\frac{l^2}{2EJ_3} - \frac{8z_{\mathrm{c}}}{\pi E' R^8}\int_{A_{\mathrm{c}}} \alpha h^2 F_2^2 dA_{\mathrm{c}}$$

$$g_{3,3} = \left(\frac{\kappa l}{GA} + \frac{l^3}{3EJ_2}\right) + \frac{32z_{\mathrm{c}}^2}{\pi E' R^8}\int_{A_{\mathrm{c}}} \alpha\beta^2 F_1^2 dA_{\mathrm{c}} + \frac{2\kappa^2(1+\nu)}{\pi E' R^4}\int_{A_{\mathrm{c}}} \alpha F_{\mathrm{III}}^2 dA_{\mathrm{c}}$$

$$g_{3,4} = \frac{2\kappa(1+\nu)}{\pi E' R^6}\int_{A_{\mathrm{c}}} \alpha h F_{\mathrm{III}}^2 dA_{\mathrm{c}}$$

$$g_{3,5} = \frac{l^2}{2EJ_2} + \frac{32z_{\mathrm{c}}}{\pi E' R^8}\int_{A_{\mathrm{c}}} \alpha\beta^2 F_1^2 dA_{\mathrm{c}}$$

$$g_{3,6} = \frac{-16z_{\mathrm{c}}}{\pi E' R^8}\int_{A_{\mathrm{c}}} \alpha\beta h F_1 F_2 dA_{\mathrm{c}}$$

$$g_{4,4} = \frac{l}{GJ_1} + \frac{8}{\pi E' R^8}\int_{A_{\mathrm{c}}} \alpha\beta^2 F_{\mathrm{II}}^2 dA_{\mathrm{c}} + \frac{2(1+\nu)}{\pi E' R^8}\int_{A_{\mathrm{c}}} \alpha h^2 F_{\mathrm{III}}^2 dA_{\mathrm{c}}$$

$$g_{5,5} = \frac{l}{EJ_2} + \frac{32}{\pi E' R^8}\int_{A_{\mathrm{c}}} \alpha\beta^2 F_1^2 dA_{\mathrm{c}}$$

$$g_{5,6} = \frac{-16}{\pi E' R^8}\int_{A_{\mathrm{c}}} \alpha\beta h F_1 F_2 dA_{\mathrm{c}}$$

$$g_{6,6} = \frac{l}{EJ_3} + \frac{8}{\pi E' R^8}\int_{A_{\mathrm{c}}} \alpha h^2 F_2^2 dA_{\mathrm{c}}$$